Research Square

Preprints are preliminary reports that have not undergone peer review.
They should not be considered conclusive, used to inform clinical practice,
or referenced by the media as validated information.

Unveiling the role of Ta in Cr-Ta-Ti modified silicide coatings for Nb alloy with superior oxidation resistance up to 1500 ℃

Hao Jiang
Northwestern Polytechnical University
Yanqiang Qiao
qyq@nwpu.edu.cn
Northwestern Polytechnical University
Weiping Zhang
Northwestern Polytechnical University
Xiping Guo
Northwestern Polytechnical University
Qifan You
Nanchang Hangkong University
Xuan Li
Sichuan University of Science and Engineering

Article

Keywords: Nb521, Silicide coating, Slurry sintering, Ta modification, High temperature oxidation resistance

Posted Date: April 9th, 2026

DOI: https://doi.org/10.21203/rs.3.rs-9197546/v1

License: This work is licensed under a Creative Commons Attribution 4.0 International License.
Read Full License

Additional Declarations: No competing interests reported.

Abstract

To address the insufficient high temperature oxidation resistance of Nb521 alloy in engineering applications, Cr-Ta-Ti modified silicide coatings with different Ta contents were fabricated on its surface via slurry sintering. The oxidation behavior and elemental diffusion characteristics of the coatings were systematically investigated at 1400–1500 ℃, and the mechanism by which Ta affects the microstructural evolution and oxidation resistance of the coatings was revealed. The results show that the Cr-Ta-Ti modified silicide coating exhibits a distinct multilayer structure, which from top to bottom consists of a (Nb,Cr,Ti,Ta)Si_2/$Cr_4Nb_2Si_5$ composite layer, a dense $NbSi_2$ layer, a $NbSi_2$/Nb_5Si_3 layer, and a Nb_5Si_3 transition layer. The introduction of Ta influences the diffusion of Si, Cr, and other elements, resulting in a reduced coating thickness. An appropriate Ta content (5Ta) can markedly decrease the growth rate of the oxide scale, providing effective protection for the substrate for at least 150 h at 1400 ℃ and 100 h at 1500 ℃, respectively. The dissolution of Ta into SiO_2 and TiO_2 enhances the high temperature viscosity and thermal stability of the oxide scale, restrains the inward diffusion of oxygen and the outward diffusion of coating elements, thereby significantly improving the high temperature oxidation resistance of the coating.

1. Introduction

To meet the urgent demands of next-generation aero-engines with high thrust-to-weight ratios and reusable spacecraft for extreme hot-section components (service temperature > 1500 ℃), developing material systems with both ultra-high temperature mechanical properties and long-term oxidation resistance has become an imperative [1, 2]. Due to their high melting points, low densities, excellent high temperature strengths, and good processability, Nb based alloys are considered ideal structural materials in the ultra-high temperature field [3–7]. Currently, Nb based alloys widely studied and applied in the aerospace sector (such as C103, Nb521, Nb-Si based alloys, and Nb-Ti-Al based alloys) inherently form expansive oxides, such as Nb_2O_5, during the oxidation process, which are detrimental to their oxidation performance [8]. Consequently, Nb based alloys must rely on compatible high temperature anti-oxidation coatings for protection when utilized in aerobic environments [9–13].

Among various coating systems, silicide coatings have emerged as one of the most extensively researched and successfully engineered protective strategies, as they can form a continuous, dense SiO_2 protective scale with an extremely low oxygen diffusion rate during high temperature oxidation [14, 15]. Early studies predominantly focused on single silicide coatings such as $MoSi_2$ and $NbSi_2$ [16, 17]. However, these generally suffer from intermediate-temperature "pesting" oxidation failure, cracking caused by coefficient of thermal expansion (CTE) mismatch with the substrate, and the decomposition and degradation of silicide phases under long-term high temperature [18]. To overcome these bottlenecks, elemental modification and structural composite design have been widely adopted to mitigate these issues [19–24]. For instance, preparing multi-element modified silicide coatings by introducing elements such as Cr, Ti, and Al can alleviate the aforementioned problems to a certain extent

[25–27]. Under ultra-high temperature service conditions, coatings face immense challenges. For example, the SiO_2 scale exhibits insufficient thermal stability at ultra-high temperature, presenting a significant risk of high temperature volatilization [28]. Furthermore, exposure to ultra-high temperature aggravates elemental interdiffusion within the coating, which can easily induce the premature decomposition of key protective phases including $NbSi_2$ and exhausts the constrained silicon reservoir within the coating [29]. In addition, the interdiffusion and degradation at the coating/substrate interface are prominent. The continuous inward diffusion of Si into the substrate not only leads to Si depletion in the coating but also forms a brittle silicide layer at the interface, acting as a mechanical weak link [30].

Introducing refractory elements or high temperature stabilizing elements is an effective approach to enhance the oxidation resistance of coatings at higher temperature [31, 32]. For example, Wang et al. [33] prepared a Y_2O_3-modified $MoSi_2$ silicide coating using supersonic atmospheric plasma spraying. Their research demonstrated that Y_2O_3 can regulate the microstructure of the generated glassy oxide scale during oxidation, thereby improving the high temperature oxidation resistance of the coating. Wang et al. [20] fabricated a $(Nb,Ti,Mo)Si_2$-$(Ti,Nb,Mo)_5Si_3$ composite coating on the surface of C103 alloy using slurry sintering method. The coating maintained its structural integrity after oxidation for 100 h at 1400 ℃ and 1500 ℃, respectively. Ta and Nb are refractory metals of the same group with similar atomic radii and chemical properties, allowing Ta to dissolve into the niobium silicide phase to form a stable solid solution [34, 35]. This solid solution effect not only strengthens the coating via lattice distortion but also draws significant attention in the field of ultra-high temperature protective coatings due to extremely high melting point (~ 3017 ℃) of Ta and superior high temperature stability. Existing studies have confirmed that Ta can dissolve into the SiO_2 glass network formed at high temperature, which not only significantly reduces the oxygen permeability of liquid SiO_2 [36] but also enhances the bond strength of Si-O bonds [37, 38]. These effects are of paramount importance for enhancing the compactness of the oxide scale and extending its long-term thermally stable service life.

However, studies also indicate that the protective performance of a single Ta-Si-O oxide scale is less than ideal. For instance, Bahr et al. [39] found that a single $TaSi_2$ coating forms a discontinuous and porous Ta_2O_5+SiO_2 mixed oxide scale at high temperature (> 850 ℃), which may conversely act as a rapid diffusion channel for oxygen ions, accelerating the coating's oxidation rate. It is evident that simple Ta substitution or addition does not consistently yield excellent protective effects and may even induce adverse impacts under certain circumstances. To overcome the shortcomings of single element modification, it is feasible to design the co-addition of Ta with metallic elements (e.g., Ti, Cr, Mo, W, Hf) or active elements (e.g., B, Y). Through the multi-element synergistic effect, it is promising to break through the performance bottlenecks of singly modified systems. Nevertheless, current research on multi-element modification mainly focuses on Cr-Ti or Mo-W systems [27, 40], and the application of Cr-Ta-Ti ternary synergistic modification in silicide coatings has not yet been reported. There is a lack of systematic experimental data and in-depth mechanistic analyses addressing key scientific issues, such as the microstructural evolution laws of multi-element modified silicide coatings and the formation mechanisms of mixed oxide scales under high temperature environments.

In view of this, the present study aims to systematically investigate the microstructure, high temperature oxidation behavior, and intrinsic mechanisms of Cr-Ta-Ti modified silicide coatings on the surface of Nb521 alloy. The Cr-Ta-Ti modified silicide coatings were successfully fabricated on the Nb521 alloy using the slurry sintering method, which is widely applied in industry. Through systematic long-term isothermal oxidation experiments at 1400 ℃ and 1500 ℃, the oxidation kinetics, microstructural evolution of the oxide scale, and coating degradation behavior before and after modification were comparatively analyzed. Emphasis was placed on the effects of Ta content on the phase formation, microstructure, and diffusion behavior of key elements (Si, Cr, Ti, Nb) in the coatings. Finally, the functional mechanisms of Ta modification on the composition, structure, adhesion, and oxygen barrier properties of the mixed oxide scale were discussed. The results of this study not only provide a new perspective for understanding the oxidation protection mechanisms of multi-element silicide coatings modified by refractory elements but also offer crucial theoretical bases and feasible technical pathways for developing long-life, highly reliable protective coatings for Nb alloys applied in extreme ultra-high temperature environments.

2. Materials and methods

2.1 Substrate material

In this work, Nb521 alloy with a nominal composition of Nb-5W-2Mo-1Zr (wt.%) was used. The alloy ingot was cut into specimens with dimensions of 15 mm × 6 mm × 3 mm using a wire electrical discharge machine. All specimen surfaces, edges and corners were gradually ground and polished with SiC sandpapers from 80# to 800# to reduce stress concentration. Subsequently, the specimens were ultrasonically cleaned in ethanol for 15 min and dried for later use.

2.2 Coating process

Pure Si powder (purity ≥ 99%, particle size 74 μm), Cr powder (purity ≥ 99.9%, particle size 2–5 μm), Ti powder (purity ≥ 99.9%, particle size 1–3 μm) and Ta powder (purity ≥ 99.95%, mesh < 325) were selected as raw materials. The corresponding powders were weighed according to the mass ratio Si:Cr:Ti:Ta = 15:4:1:x (x = 0, 5, 10, 15), mixed with ethanol and polyvinyl butyral (PVB), and ball milled for 4 h to prepare a uniform slurry. For convenience, the Cr-Ta-Ti modified silicide coatings with different Ta contents are denoted as 0Ta, 5Ta, 10Ta and 15Ta, respectively.

The pretreated substrate specimens were immersed in the slurry for 3–5 s, taken out and dried in air for 10–15 min, and this process was repeated three times. The coated specimens were dried in a vacuum oven at 100 ℃ for 4 h. Finally, all samples were sintered at 1450 ℃ for 0.5 h in an ultra-high vacuum furnace and then cooled to room temperature with the furnace.

2.3 Oxidation test

Isothermal oxidation tests were carried out in a muffle furnace at 1400 ℃ and 1500 ℃ for 1-150 h. After oxidation, the samples were directly taken out of the furnace and cooled naturally in air. The mass

changes before and after oxidation were measured using an electronic balance with an accuracy of 0.1 mg

2.4 Analyzing methods

Scanning electron microscopy equipped with energy-dispersive X-ray spectroscopy (SEM/EDS, TESCAN MIRA 3 and Inca X-sight) and X-ray diffraction (XRD, Panalytical X'Pert PRO, Cu Kα) were employed to analyze the microstructure, phase composition and elemental distribution of the samples before and after oxidation. Elemental distribution of the samples was characterized by electron probe microanalysis (EPMA).

3. Results

3.1 Microstructure of the Cr-Ta-Ti modified silicide coating

Figure 1 and 2 show the surface XRD patterns and surface BSE images of the Cr-Ta-Ti modified silicide coatings with different Ta contents, respectively. According to the XRD analysis results, all coatings are mainly composed of the $NbSi_2$ phase and a small amount of the $Cr_4Nb_2Si_5$ phase. As seen from the surface images of the coatings (Fig. 2), with the increase of Ta content, the surface roughness of the coatings gradually increases, and the number of pores also increases accordingly. After the addition of Ta, a white Ta-rich phase (Sites 3 and 4 in Fig. 2) appears on the coating surface, which remains the $NbSi_2$ phase. Furthermore, a small amount of incompletely reacted residual slurry can be observed in the samples, as indicated by Site 6 in Fig. 2d and EDS composition in Table 1.

(a) 0Ta, (b) 5Ta, (c)10Ta and (d)15Ta.

Table 1
Chemical compositions of the marked sites in Fig. 2, determined by EDS.

Sites	Composition (at.%)				
	Si	Nb	Cr	Ti	Ta
1	69.9	21.2	5.8	3.1	-
2	71.7	18.3	5.9	3.6	0.5
3	66.0	19.5	8.5	3.3	2.7
4	69.7	12.6	9.7	3.7	4.3
5	69.6	17.4	8.7	3.8	0.5
6	44.4	4.2	23.1	13.0	15.3
7	67.4	23.1	4.3	3.8	1.4

Figure 3 presents the cross-sectional BSE morphologies of the Cr-Ta-Ti modified silicide coatings with different Ta contents. There is no significant difference in the overall structure of all coatings, which are composed of two layers: a main layer and a transition layer. The main layer can be further divided into two sub-layers: the upper layer consists of a gray phase and a dispersed dark-gray granular phase, while the lower layer is a single gray phase. Combining the EDS compositional analysis (Table 2) and XRD results (Fig. 1), it can be determined that the upper gray phase is the (Nb,Cr,Ti,Ta)Si_2 phase (Sites 1, 2, 6, and 7 in Table 2). Moreover, as the Ta content increases, the Ta concentration in the (Nb,Cr,Ti,Ta)Si_2 phase increases synchronously, albeit with a limited increment. The dispersed dark-gray phase is identified as the $Cr_4Nb_2Si_5$ phase (Site 3 in Table 2). The lower single gray phase is the $NbSi_2$ phase (Site 4 in Table 2), and the transition layer is composed of Nb_5Si_3 phase. Between the single $NbSi_2$ layer and the Nb_5Si_3 layer, a mixed layer composed of $NbSi_2$+Nb_5Si_3 is found. Evidently, the coating consists of a (Nb,Cr,Ti,Ta)Si_2+$Cr_4Nb_2Si_5$ layer, a single $NbSi_2$ layer, a $NbSi_2$+Nb_5Si_3 mixed layer, and a Nb_5Si_3 transition layer from top to bottom. It is noteworthy that the coating thickness gradually decreases with the increase of Ta content. The thicknesses of the main layers for the 0Ta, 5Ta, 10Ta, and 15Ta coatings are approximately 122, 113, 90, and 77 μm, respectively.

Table 2
Chemical compositions of the marked sites in Fig. 3, determined by EDS.

Sites	Composition (at.%)				
	Si	Nb	Cr	Ti	Ta
1	68.7	20.6	6.9	3.8	-
2	69.9	22.7	5.0	1.2	1.2
3	48.0	13.2	33.7	5.1	-
4	67.7	32.3	-	-	-
5	38.4	61.6	-	-	-
6	66.7	26.1	4.2	1.2	1.8
7	68.3	22.7	4.4	2.6	2.0

Figure 4 displays the cross-sectional BSE image of 5Ta coating and the elemental mapping of the corresponding region. It can be seen that the Nb element exhibits a three-layer distribution in the coating above the substrate. The bottom most part of the coating, which has a lower Si content, is the Nb_5Si_3 transition layer, above which lies the $NbSi_2$ and Nb_5Si_3 mixed layer. The Si and Nb elements are distributed uniformly in the single $NbSi_2$ layer. There is a distinct Cr-enriched region in the upper layer of the coating, primarily corresponding to the $Cr_4Nb_2Si_5$ phase. The Ti element is also enriched here and is mainly distributed in the upper layer of the coating. The Ta element is distributed relatively uniformly

throughout the coating, but its content is relatively higher within the range from the coating surface down to 30 μm. Mo, W, and Zr are substrate elements and are mainly concentrated in the substrate.

3.2 Oxidation behavior of the coating

3.2.1 Oxidation kinetics

The mass changes per unit area of the Cr-Ta-Ti modified silicide coatings with different Ta contents after oxidation at 1400 ℃ and 1500 ℃ are shown in Fig. 5. The 0Ta coating exhibits a characteristic of continuous weight loss during oxidation at 1400 ℃, whereas 5Ta coating only shows a slight weight gain in the early stage of oxidation and also experiences weight loss in the later stage. After 150 h of oxidation, there is no significant difference in the mass change per unit area between the two coatings. The oxidation weight gain of 10Ta and 15Ta coatings increases sharply, indicating that the coatings have failed. Under the 1500 ℃ oxidation condition, the specific oxidation weight gain of 0Ta coating first drops significantly and then turns to a slow increase after 10 h of oxidation, with a mass change per unit area of 1.2 mg/cm² at 100 h. The 5Ta coating initially shows a weight gain, begins to continuously lose weight after 5 h, and slowly recovers after 50 h, resulting in a mass change per unit area of -0.3 mg/cm² after 100 h of oxidation.

Figure 6 illustrates the macroscopic morphologies and the corresponding BSE images of the failure regions for the Cr-Ta-Ti modified silicide coatings with different Ta contents after oxidation at 1400 ℃ and 1500 ℃. Obviously, after 50 h of oxidation at 1400 ℃, a large amount of oxides of the substrate element Nb appears on the surface of 15Ta coating (Fig. 6d), and its specific oxidation weight gain increases sharply (Fig. 5a), indicating coating failure. This can probably be attributed to the relatively thin thickness of 15Ta coating, making it difficult to provide long-term protection for the substrate under high temperature conditions. After 50 h of oxidation, the coating has essentially degraded completely, generating a large amount of non-protective oxides (Nb_2O_5), leading to the loss of protective capability. After oxidation at 1400 ℃ for 100 h (Fig. 5c), the surface of 10Ta coating also generates a substantial amount of white Nb_2O_5 products. Combined with the cross-sectional observation of the coating, these oxides grow outward from the interior of the substrate, and the substrate has undergone obvious oxidation, resulting in the destruction of the coating structure. In contrast, the overall structures of the 0Ta and 5Ta coatings remain relatively intact after long-term isothermal oxidation. For 0Ta coating, after 150 h of oxidation at 1400 ℃, its surface exhibits a yellowish-brown appearance with dark-brown spots in localized regions. Microstructural characterization reveals the presence of a large number of mixed oxide particles of Nb_2O_5 and TiO_2 in the dark-brown regions. At this point, the coating has essentially failed, and obvious cracks are observed at the coating/substrate interface. A mixed oxide scale of SiO_2-Nb_2O_5-TiO_2 with a thickness of approximately 27.3 μm has formed on the coating surface. After further oxidation at 1500 ℃ for 100 h, the entire surface of 0Ta coating turns yellowish-brown. After oxidation at 1400 ℃, the surface of 5Ta coating is entirely brown, while after oxidation at 1500 ℃, its surface is completely covered by a dense glassy dark-brown oxide scale.

3.2.2 Oxidation products

Figure 7 shows the XRD patterns of 5Ta coating after oxidation at different temperature for different time. After oxidation, the phase composition of the coating surface is mainly $NbSi_2$, SiO_2, Cr_2O_3 and TiO_2. At 1400 ℃ and 1500 ℃, the oxidation products of the coating are primarily SiO_2, Cr_2O_3, and TiO_2. With prolonged oxidation time, the diffraction peaks of SiO_2 and TiO_2 gradually intensify, whereas those of Cr_2O_3 show a weakening trend. No diffraction peaks of Nb_2O_5 and Ta_2O_5 are detected throughout the entire oxidation process.

3.2.3 Microstructure of the coating oxidized at 1400 ℃

Table 3
Chemical compositions of the marked sites in Fig. 8, determined by EDS.

Sites	Composition (at.%)					
	Si	Nb	Cr	Ti	Ta	O
1	2.7	-	32.6	0.5	-	64.2
2	27.7	9.0	2.1	1.7	-	59.5
3	16.5	5.1	4.7	10.5	-	63.2
4	25.8	3.4	0.5	2.0	-	68.3
5	1.0	1.0	0.6	18.1	-	79.3
6	26.6	-	-	1.6	-	71.8
7	2.5	1.4	1.5	15.1	1.8	77.7

Figure 8 presents the surface BSE images of 5Ta coating after oxidation at 1400 ℃ for different time. As can be seen from Fig. 8a, after 1 h of oxidation, the oxide scale formed on the coating surface is not dense. Combining the XRD analysis results (Fig. 7) and the EDS data at Site 1 (Fig. 8 and Table 3), the oxides formed on the coating surface are mainly Cr_2O_3. This indicates that during the oxidation process, the Cr element continuously diffuses outward and reacts with oxygen. When the oxidation time was extended to 5 h, white granular TiO_2 begins to appear on the coating surface (Site 3 in Fig. 8 and Table 3). Simultaneously, the content of SiO_2 (Site 4 in Fig. 8 and Table 3) also increases significantly. Obviously, the content of the Cr_2O_3 phase formed on the coating surface in the early stage of oxidation gradually decreases, which is due to the transformation of Cr_2O_3 into volatile CrO_3 at high temperature (Figs. 7 and 8) [41, 42]. As oxidation time extends, the oxide scale formed on the coating surface gradually becomes denser and more compact. When the oxidation time reaches 20 h, the coating surface is completely covered by a dense oxide scale. This oxide scale mainly consists of SiO_2 and fine TiO_2 particles dispersed within it. At this stage, the intrusion rate of oxygen into the substrate is

drastically reduced, leading to a significant decrease in the oxidation rate. In the later stage of oxidation, the surface products of the coating remain basically unchanged, mainly composed of SiO_2 and TiO_2. Furthermore, with the further extension of oxidation time, both the content and size of the TiO_2 particles on the coating surface exhibit a continuously increasing trend. Additionally, the EDS compositional analysis at Site 7 in Fig. 8 (Table 3) reveals that the TiO_2 particles contain small amounts of Cr and Nb, indicating that the Cr and Nb elements exist in the TiO_2 particles in the form of a solid solution.

Table 4
Chemical compositions of the marked sites in Fig. 9, determined by EDS.

Sites	Composition (at.%)					
	Si	Nb	Cr	Ti	Ta	O
1	-	-	40.2	-	-	59.8
2	69.9	22.7	1.2	5.0	1.2	-
3	24.9	4.7	3.2	0.9	0.3	66.0
4	24.6	1.9	-	0.7	-	72.8
5	63.2	28.2	5.8	2.8	-	-
6	37.3	33.1	25.8	3.8	-	-
7	67.2	32.8	-	-	-	-
8	4.3	-	23.8	9.4	-	62.5
9	46.3	30.6	16.4	6.7	-	-
10	5.0	12.4	15.3	3.1	-	64.2
11	68.6	31.4	-	-	-	-
12	46.5	46.0	7.5	-	-	-
13	63.5	36.5	-	-	-	-
14	38.2	59.5	2.3	-	-	-

Figure 9 shows the cross-sectional BSE images of 5Ta coating after oxidation at 1400 ℃ for different time. Similar to the variation pattern of the coating surface, after 1 h of oxidation, the pore regions on the coating surface are filled with a large amount of Cr_2O_3 (Site 1 in Fig. 9). At this time, the overall structure of the coating has not undergone obvious alterations, and the $Cr_4Nb_2Si_5$ phase can be clearly identified from the locally magnified morphology (Site 3 in Fig. 9). As the oxidation time extends to 5 h, the oxide content on the coating surface further increases, while the $Cr_4Nb_2Si_5$ phase gradually decreases. Meanwhile, a white degradation region is observed between the (Nb,Cr,Ti,Ta)Si_2 layer and the single

$NbSi_2$ layer (Fig. 9c). With further extension of the oxidation time, the content of SiO_2 formed on the coating surface continuously increases (Site 4 in Fig. 9), and the white degradation region inside the coating further expands, which is mainly composed of $(Nb,Cr,Ti)_5Si_3$ phase (Table 4). Upon oxidation to 20 h, the coating surface is essentially covered by a continuous oxide scale, within which Cr_2O_3 embedded in SiO_2 can still be observed (Site 8 in Fig. 9). At this stage, the coating has undergone significant degradation, and a two-phase region of $(Nb,Cr,Ti,Ta)Si_2/(Nb,Cr,Ti)_5Si_3$ can be observed beneath the $(Nb,Cr,Ti,Ta)Si_2$ layer. As the oxidation time continues to prolong, the oxide scale on the coating surface continuously thickens, and the $(Nb,Cr,Ti)_5Si_3$ degradation region also expands continuously. Conversely, the $(Nb,Cr,Ti,Ta)Si_2$ layer and the single $NbSi_2$ layer continuously degrade and decrease. After 150 h of oxidation, a dense oxide scale with a thickness of approximately 22 μm has formed on the coating surface, which is mainly composed of SiO_2, TiO_2, and Cr_2O_3 (Site 10 in Fig. 9). Notably, the dissolved Cr, Ti, and Ta atoms in the original $(Nb,Cr,Ti,Ta)Si_2$ layer can no longer be detected (Site 11 in Fig. 9). This indicates that during the long-term oxidation process, the Cr, Ti, and Ta elements continuously diffuse outward and undergo oxidation reactions, thereby driving the gradual transformation of the $(Nb,Cr,Ti,Ta)Si_2$ phase into the pure $NbSi_2$ phase.

3.2.4 Microstructure of the coating oxidized at 1500 ℃

Figure 10 shows the surface BSE images of 5Ta coating after oxidation at 1500 ℃ for different time. After 1 h of oxidation, the coating surface was immediately covered by a large amount of Cr_2O_3, while abundant pore defects still remained. With prolonged oxidation time, the content of Cr_2O_3 on the coating surface gradually decreased, whereas that of SiO_2 exhibited an increasing trend. When the oxidation time reached 20 h, Cr_2O_3 was barely detectable on the surface, which was fully covered by a continuous glassy SiO_2 layer. In addition, the content of TiO_2 embedded in the SiO_2 matrix also increased gradually. With further extension of oxidation time, the surface oxide scale became progressively denser, and both the content and size of TiO_2 particles increased. The morphological evolution of the scale was generally consistent with that observed at 1400 ℃.

Figure 11 shows the cross-sectional BSE images of 5Ta coating after oxidation at 1500 ℃ for different time. After 1 h of oxidation, the coating surface was covered by a Cr_2O_3 layer with a thickness of approximately 3 μm. When oxidized for 5 h, a considerable amount of SiO_2 phase was formed on the coating surface besides Cr_2O_3. At this stage, a $(Nb,Cr,Ti)_5Si_3$ degraded layer with a thickness of about 15 μm was observed in the coating. After 10 h of oxidation, the Cr_2O_3 content on the coating surface decreased remarkably. The coating from top to bottom consisted of a mixed SiO_2-TiO_2-Cr_2O_3 oxide scale, a $(Nb,Cr,Ti,Ta)Si_2$ layer, a $(Nb,Cr,Ti)_5Si_3$ layer, a single $NbSi_2$ layer, and a Nb_5Si_3 layer. With further oxidation up to 20 h, the scale thickened continuously and was mainly composed of SiO_2 and TiO_2. Similar to the oxidation behavior at 1400 ℃, both the $(Nb,Cr,Ti,Ta)Si_2$ layer and the single $NbSi_2$ layer degraded continuously and reduced in content. After 100 h of oxidation, the single $NbSi_2$ layer was completely depleted, and $(Nb,Cr,Ti,Ta)Si_2$ was fully transformed into pure $NbSi_2$ (Fig. 11f).

To investigate the elemental diffusion behavior during high temperature oxidation, EPMA elemental mapping was performed on the cross-section of 5Ta coating after oxidation at 1500 ℃ for 1 h and 100 h, as shown in Figs. 12 and 13, respectively. As can be seen from Fig. 12, after oxidation at 1500 ℃ for 1 h, Nb and Si in the coating exhibited a three-layered distribution, corresponding to the (Nb,Cr,Ti,Ta)Si_2/$Cr_4Nb_2Si_5$ layer, the single $NbSi_2$ layer, and the Nb_5Si_3 layer. Cr was mainly distributed in $Cr_4Nb_2Si_5$ phase and was significantly enriched in the surface oxide. Notably, the overall Cr concentration in the coating was considerably lower than that before oxidation (Fig. 4). Ti was primarily concentrated in the (Nb,Cr,Ti,Ta)Si_2/$Cr_4Nb_2Si_5$ layer. O was mainly enriched in the surface oxide, while Ta was predominantly distributed in the upper (Nb,Cr,Ti,Ta)Si_2 phase, with a small amount also detected in the surface oxide scale. W, Mo, and Zr were mostly retained in the substrate.

As shown in Fig. 13, after oxidation at 1500 ℃ for 100 h, the thickness of the scale increased substantially. Compared with the 1 h oxidized sample, the Si content in the residual coating decreased sharply, indicating significant outward diffusion of Si. Meanwhile, the Cr and Ti contents in the coating were obviously reduced. Ti was enriched in the scale as TiO_2, in which the enrichment of Nb and Cr could also be detected, suggesting that a certain amount of Nb and Cr was dissolved in TiO_2. In addition, Ta was also enriched in the TiO_2 phase and was prominently distributed in the white degraded Nb_5Si_3 phase in the upper residual coating. It is worth noting that W and Mo were significantly enriched at the coating transition layer/substrate interface.

4. Discussion

4.1 Formation mechanism of Cr-Ta-Ti modified silicide coating

A schematic diagram illustrating the formation mechanism of the Cr-Ta-Ti modified silicide coating is displayed in Fig. 14. Due to the low melting point of Si (< 1420 ℃) [43] and its high mass fraction of 75 wt% in the slurry, Si melted rapidly to form a liquid phase when the sintering temperature exceeded its melting point. Therefore, the coating formation was mainly dominated by the inward diffusion of liquid Si into the substrate.

At the initial stage of reaction, liquid Si came into contact with the Nb substrate and reacted rapidly to produce a Nb_5Si_3 transition layer. Subsequently, Nb_5Si_3 further reacted with the inward-diffusing Si and transformed into $NbSi_2$. Driven by the Si concentration gradient, this reaction front continuously propagated toward the substrate interior. Meanwhile, Cr, Ti, and part of Ta in the slurry also participated in the reaction. Cr and Ti diffused inward together with Si and dissolved into the as-formed $NbSi_2$ lattice driven by the concentration gradient. With the reaction proceeding, the coating thickness increased rapidly. Since the solid solubility of Cr in $NbSi_2$ was limited [44], $Cr_4Nb_2Si_5$ precipitated as a secondary phase when the local Cr content exceeded its solubility limit. In contrast, Ti remained dissolved in $NbSi_2$ owing to its relatively low content. Eventually, the coating exhibited a typical four-layered structure from

top to bottom: a mixed (Nb,Cr,Ti,Ta)Si_2/$Cr_4Nb_2Si_5$ layer, a single $NbSi_2$ layer, a $NbSi_2$/Nb_5Si_3 layer, and a Nb_5Si_3 transition layer.

Notably, increasing the Ta content in the slurry did not significantly improve the dissolved Ta concentration inside the coating (sites 6 and 7 in Fig. 3). This phenomenon is mainly attributed to the kinetic constraints of diffusion. Firstly, due to its relatively large atomic radius [45], Ta exhibits substantially higher diffusion resistance in silicide lattices and grain boundaries in comparison with Cr and Ti, which in turn leads to a slower migration rate toward the substrate. Secondly, as a high melting point refractory metal, Ta exhibits a significantly lower thermal diffusivity at the sintering temperature of 1450 ℃ than Cr and Ti, which are close to a molten state [46, 47]. This indicates that the diffusion of Ta acts as the rate-limiting step in the present sintering system. Simply increasing the Ta content in the slurry cannot overcome its diffusion kinetic barrier. Instead, excessive unreacted Ta tends to accumulate in the upper coating, hindering the effective diffusion of Si and other active elements and eventually reducing the coating thickness (Fig. 3).

4.2 Oxidation mechanism of Cr-Ta-Ti modified silicide coating

Based on the above analysis of oxidation kinetics and oxide scale evolution, the oxidation process of the Cr-Ta-Ti modified silicide coatings can be divided into three stages. At the initial oxidation stage (1–5 h), oxygen reacts with (Nb,Cr,Ti,Ta)Si_2 on the coating surface, rapidly forming amorphous SiO_2. Meanwhile, driven by the concentration gradient, a large amount of Cr diffuses outward and reacts with oxygen to form Cr_2O_3. EPMA elemental mapping (Fig. 12) confirms that most Cr_2O_3 is distributed at the coating pores at this stage. In addition, a small amount of Ta is uniformly distributed in the oxide scale without forming discrete oxide particles of Ta, and no diffraction peaks of Ta_2O_5 are observed in the XRD patterns (Fig. 7). This indicates that Ta is incorporated into the SiO_2 glass network in the form of solid solution during oxidation. Previous studies have demonstrated that Ta ion doping can significantly improve the high temperature viscosity of the SiO_2 glass phase and effectively reduce the diffusion coefficient of oxygen ions in the SiO_2 glass network [48, 49]. Such an in-situ modification effect endows the as-formed oxide scale with favorable compactness and oxygen barrier properties, suppressing the rapid inward penetration of oxygen. Although Cr tends to diffuse outward and form volatile Cr_2O_3, the Ta-doped high viscosity oxide scale can inhibit the excessive volatilization of Cr to a certain extent, maintaining a more intact oxide scale structure.

At the middle oxidation stage (5–20 h), the further oxidative volatilization of Cr_2O_3 at high temperatures (especially 1500 ℃) and the increased formation of SiO_2 become the dominant factors controlling the oxidation behavior. As seen from the oxidation kinetic curves (Fig. 5b), the coating without Ta shows a remarkable mass gain during the middle oxidation stage, whereas the mass change of the 5Ta coating continues to decrease slowly. In this system, the mass gain is attributed to the reaction between the silicide coating and oxygen to form oxides, while the mass loss results from the continuous further

oxidation and volatilization of Cr_2O_3. The difference in oxidation kinetics reveals that the oxidation rate of the 5Ta coating is lower than that of the Ta-free coating, which is mainly ascribed to two reasons. First, the SiO_2 oxide scale doped with Ta exhibits superior high temperature thermal stability compared with pure SiO_2. Its viscosity is less affected by temperature fluctuations, enabling it to effectively cover the microporous defects left by Cr_2O_3 volatilization and showing excellent self-healing ability. Second, Ta dissolved in the SiO_2 glassy oxide scale acts as a skeleton-strengthening component, which improves the overall corrosion resistance of the oxide scale [50] and reduces the oxidation rate. Accordingly, the SiO_2-Cr_2O_3 mixed oxide scale formed at this stage is denser than that of the unmodified coating, which can effectively block the oxygen transport pathways. This is consistent with the experimental results of the significantly reduced oxidation mass gain rate (Fig. 5) and the decreased oxide scale thickness (Fig. 15) [51]. However, the advantage of the 5Ta coating in the oxidation kinetic curve is not obvious at 1400 ℃, indicating that the effect of refractory Ta cannot be fully exerted at relatively low temperatures. The higher the temperature, the more significantly Ta functions.

At the late oxidation stage (20–100 h), the coating undergoes continuous degradation. The high-silicide layer gradually degrades due to the sustained diffusion and consumption of Si. Once this layer is completely depleted, the coating will lose its protective capability and fail because sufficient Si can no longer be supplied to the surface layer. Therefore, a sufficient coating thickness is required to achieve long-term protection of the substrate in high-temperature oxidation environments. The 10Ta and 15Ta coatings are prone to failure during this stage (Fig. 5), with insufficient thickness being a major contributing factor. In contrast, for the 5Ta coating, even after oxidation at 1500 ℃ for 100 h, the $NbSi_2$ layer still retains a thickness of 23.7 μm (Fig. 11), and the coating surface is completely covered by a mixed SiO_2-TiO_2-Cr_2O_3 oxide scale with a thickness of approximately 27.4 μm. The mixed oxide scale on the coating surface can significantly suppress the inward diffusion of oxygen, and the silicide beneath the oxide scale can continuously supply Si to the outer layer. From the distribution of Ta at the late oxidation stage, obvious enrichment of Ta in TiO_2 is observed. It has been reported [34] that the introduction of Ta leads to the substitution of tetravalent Ti by pentavalent Ta, which reduces the concentration of Ti vacancies and O vacancies in TiO_2, thereby inhibiting the inward diffusion of oxygen and the outward diffusion of Ti. This indicates that the defect reaction triggered by Ta^{5+} entering the TiO_2 lattice effectively reduces the overall concentration of Ti vacancies and O vacancies in TiO_2. Since oxygen vacancies serve as the main diffusion pathways for oxygen ions in oxides, their markedly decreased concentration directly hinders the diffusion rate of oxygen ions through TiO_2 grains or grain boundaries. Meanwhile, the reduced point defects render the TiO_2 solid solution grains more structurally intact and denser, further enhancing the thermal stability and oxygen diffusion barrier property of this oxide. In addition, the stable Ta-O structure exerts a pinning effect in the oxide scale, suppressing the excessive flow and structural relaxation of the SiO_2 glass phase at ultra-high temperatures, and ensuring the structural integrity of the oxide scale during long-term service. Accordingly, at the late stage, Ta improves the overall protective performance of the coating through the above mechanisms, leading to a significantly reduced oxide scale thickness (Fig. 15).

By comparative analysis with the Cr-Ti modified silicide coating without Ta addition [51], the introduction of Ta optimizes the formation process, microstructure, and high temperature stability of the oxide scale at 1400 ℃ and 1500 ℃. Although the two coatings share the same oxidation stage division (dominated by Cr in the early stage and Si in the later stage), the addition of Ta significantly enhances the protective efficiency of the coating via its unique thermodynamic and kinetic effects, as directly evidenced by the obviously reduced oxide scale thickness. In summary, the core high temperature oxidation mechanism of the Cr-Ta-Ti modified silicide coating lies in achieving longer-lasting protection with a thinner and denser oxide scale by increasing the oxide scale viscosity, restraining elemental diffusion, and forming an oxide scale with low oxygen permeability. This mechanism significantly improves the oxidation resistance of the coating under extreme conditions at 1400 ℃ and 1500 ℃.

5. Conclusions

(1) The Cr-Ta-Ti modified silicide coatings exhibit a distinct layered structure, which from top to bottom consists of a (Nb,Cr,Ti,Ta)Si_2/$Cr_4Nb_2Si_5$ composite layer, a dense $NbSi_2$ layer, a $NbSi_2$/Nb_5Si_3 layer and a Nb_5Si_3 transition layer. The introduction of Ta suppresses the diffusion of Si and other active elements during sintering, resulting in a reduced total coating thickness.

(2) The addition of an appropriate amount of Ta can significantly slow down the growth rate of the oxide scale. Specifically, the 5Ta coating achieves the optimal comprehensive performance, providing effective protection to the substrate for at least 150 h at 1400 ℃ and 100 h at 1500 ℃. Coatings with an excessively high Ta content are prone to spallation failure during oxidation, and the insufficient coating thickness is one of the primary factors inducing this failure behavior.

(3) The oxidation process of the Cr-Ta-Ti modified silicide coating is controlled by the diffusion of Cr and Si. Ta “pinned” in SiO_2 and TiO_2 not only significantly improves the high temperature viscosity of the oxide scale, but also effectively inhibits the inward diffusion of oxygen ions and the outward diffusion of other elements. This dual mechanism significantly reduces the oxide scale thickness and thereby enhances the oxidation resistance of the coating.

Declarations

Author Contribution

Hao Jiang: Writing - original draft, Validation, Investigation, Data curation. Yanqiang Qiao: Writing – review & editing, Validation, Su pervision, Resources, Conceptualization. Weiping Zhang: Validation, Investigation. Xiping Guo: Writing – review & editing, Supervision. Qifan You: Investigation, Supervision. Xuan Li: Writing – review & editing, Supervision, Methodology.

Acknowledgement

This work was financially supported by the National Natural Science Foundation of China (No. 52571099), the Key R&D Program of Jiangxi Province (No. 20261BCE310021), the Key R&D Program of Xianyang (L2025-ZDYF-KTH-001) and the General Project of Sichuan Provincial Natural Science Foundation (No. 2026NSFSC0331).

References

1. Guo L, He WT, Chen WB, Xue ZL, He J, Guo YQ, Wu Y, Gao LH, Li DQ, Zhang Z, Wei LL, Gao YY, Zhang TH, Qiao J, Li QH, Guo HB (2023) Progress on high-temperature protective coatings for aero-engines. Surf Sci Technol 4:1
2. Liu YK, Liu Z, Fei YJ, Wang CH, Yang HR (2025) Study on the effect of multi-rare-earth-doping on thermal barrier coatings' thermophysical and fluorescence properties. Surf Sci Technol 3:40
3. Zhang YY, Fu T, Yu LH, Cui KK, Wang J, Shen FQ, Zhang X, Zhou KC (2023) Anti-corrosion coatings for protecting Nb-based alloys exposed to oxidation environments: A review. Met Mater Int 29:1-17
4. Chen DZ, Zhu JQ, Gong WT, Zhang XF, Xu C, Wang S, Wang QB, Xu Q, Wang Q, Chen RR, Fu HZ (2026) Combined effect of $NdNbTiO_6$ precipitation and fine microstructure on oxidation resistance of Nb-Si alloys at 1250 ℃. Corros Commun, doi: https://doi.org/10.1016/j.corcom.2026.03.011
5. Zhang X, Fu T, Cui KK, Zhang YY, Shen FQ, Wang J, Yu LH, Mao HB (2021) The protection, challenge, and prospect of anti-oxidation coating on the surface of niobium alloy. Coatings 11:742
6. Joshi K, Kumar P (2024) Strength behavior of niobium-based refractory systems. JOM 76:6277-6301
7. Tang XH, Zhao G, Liu J, Wang Q, Bai XD, Wang LF (2024) High-temperature antioxidant silicate coating of low-density Nb-Ti-Al alloy: A review. High Temp Mater Processes 43: 20240029
8. Majumdar S, Kishor J, Paul B, Hubli RC, Chakravartty JK (2015) Isothermal oxidation behavior and growth kinetics of silicide coatings formed on Nb-1Zr-0.1C alloy. Corros Sci 95:100-109
9. Narita T, Kato Y, Narita T, Ara M (2023) Advances in diffusion barrier coatings for high-temperature applications. High Temp Corros Mater 100:399-411
10. Chen DZ, Gong WT, Xu C, Zhang YJ, Hao R, Yang ZB, Chen RR, Fu HZ (2025) Oxidation behavior of Ge-modified Nb-Si alloys at 1250 ℃: Self-generated $NbGe_2$ layer with enhanced oxidation resistance. Appl Sur Sci Advances 30:100874
11. Fu T, Zhan SR, Zhang YY, Shen FQ, Wang H (2025) Preparation of Si-rich $NbSi_2$ coating on Nb surface by hot dip silicon-plating technology to improve the high-temperature oxidation resistance of pure Nb substrate. Ceram Int 51:23341-23353
12. Wang XY, Zhu L, Yang YJ, Zhang BJ, Kiryukhantsev-Korneev PV, Levashov EA, Ren XR, Ji X, Feng PZ, Wang XH (2025) Upcycling waste $MoSi_2$ into high-performance composite coatings for protecting refractory alloys across a wide temperature range. Int J Refract Met Hard Mater 132:107295
13. Xu BB, Guo XP, Qiao YQ (2024) Effects of TiB_2 contents on the microstructure and oxidation behavior of Mo-Si-B composite coatings. J Alloys Compd 1005:175967

14. Majumdar S, Sharma IG (2011) Oxidation behavior of $MoSi_2$ and $Mo(Si,Al)_2$ coated Mo-0.5Ti-0.1Zr-0.02C alloy. Intermetallics 19:541-545
15. Choi YJ, Yoon JK, Kim GH, Yoon WY, Doh JM, Hong KT (2017) High temperature isothermal oxidation behavior of $NbSi_2$ coating at 1000-1450 ℃. Corros Sci 129:102-114
16. Li LF, Guo XP, Qiao YQ (2023) Formation and oxidation resistance of $MoSi_2$ coating for Nb-Si based alloy prepared by slurry sintering method. J Alloys Compd 938:168456
17. Alam MZ, Rao AS, Das DK (2010) Microstructure and high temperature oxidation performance of silicide coating on Nb-based alloy C-103. Oxid Met 73:513-530
18. Li Z, Zhang P, Li X, Chen C, He Y, Feng P (2025) A comparison of multi-component silicide $(Ta,Mo,W)Si_2$ coatings on Nb alloy prepared by low-temperature reactive sintering using different powder feedstocks. Mater Today Commun 42:111338
19. Shao W, Cui YW, Zhou CG (2019) Diffusion paths of silicide coatings on Nb-Si-based alloys during pack cementation process. Metall Materi Trans A 50A:2945-2955
20. Wang X, Zhang W, Wang TY, Yang T, Han CX, Yang F (2025) In-situ formation mechanism and long-term isothermal oxidation behaviors at 1400 ℃ and 1500 ℃ of $(Nb,Ti,Mo)Si_2$-$(Ti,Nb,Mo)_5Si_3$ biphasic compositionally-complex ceramic composite coating on C103 alloy. Corros Sci 251:112914
21. Zhang YF, Xiao LR, Zeng DL, Li X, Zhou XJ, Zhao G, He WK, Li S, Xiao YX, Zhao XJ, Liu SA, Cai ZY (2022) A novel niobium based oxidation protective coating with three lines of defense at ultra-high temperature. Corros Sci 206: 110515
22. Ge YL, Wang YM, Chen JC, Zou YC, Guo LX, Ouyang J, Jia DC, Zhou Y (2018) An Nb_2O_5-SiO_2-Al_2O_3/$NbSi_2$/Nb_5Si_3 multilayer coating on Nb-Hf alloy to improve oxidation resistance. J Alloys Compd 745:271-281
23. Wang Z, Wang YM, Wang SQ, Zou YC, Chen GL, Wen L, Ouyang JH, Jia DC, Zhou Y (2022) $ZrSi_2$/SiO_2-Nb_2O_5/$NbSi_2$ multi-layer coating formed on niobium alloy by HAPC combined with LPDS: Microstructure evolution and high temperature oxidation behavior. Corros Sci 206:110460
24. Wang Z, Wang YM, Wang SQ, Zou YC, Chen GL, Wen L, Zhang GX, Zhao LN, Ouyang JH, Jia DC, Zhou Y (2022) Design and preparation of $MoSi_2$/SiO_2-Nb_2O_5/$NbSi_2$ multilayer coating on Nb alloy: Microstructure and hot corrosion behavior. Corros Sci 209:110733
25. Jiang H, Qiao YQ, Zhang WP, Guo XP (2024) Characterization of microstructure and oxidation behavior of Al modified $MoSi_2$ coating on Nb-Si based alloy. Surf Interfaces 51:104739
26. Li LF, Guo XP, Qiao YQ (2023) A novel composite Si-Mo-Ti coating with Ti concentration gradient for Nb-Si based ultrahigh temperature alloy prepared by slurry sintering. Corros Sci 225:111632
27. An DY, Liu CF, Zhao S, Zhang HP, Zou YC, Tang ZW, Xiao P, Dai JM, Wang YM (2023) High-temperature oxidation resistance performance of Si-Ti-Cr silicide coating on Nb-Hf alloy surface in constant oxidation and thermal shock. Rare Met Mater Eng 52:1219-1226
28. Cheng CY, Xie W, Li HJ, Fu QG (2021) Evaporation behavior of SiO_2 glass doped with various transition metal oxides. J Am Ceram Soc 104:3130-3138

29. Li JL, Wang W, Zhou CG (2017) Oxidation and interdiffusion behavior of a germanium-modified silicide coating on an Nb-Si-based alloy. Int J Miner Metall Mater 24:289-296
30. Sankar M, Prasad VVS, Baligidad RG, Alam MZ, Das DK, Gokhale AA (2015) Microstructure, oxidation resistance and tensile properties of silicide coated Nb-alloy C-103. Mat Sci Eng. A-struct 645:339-346
31. Wu JH, Wu WX, Sun AY, Zhu JY, Tang HQ, Shen F, Lei SY (2025) Study on high temperature oxidation resistance of $HfSi_2$ modified $MoSi_2$ coating. J Mater Res Technol 37:242-251
32. Ou HK, Liu YF, Fan KF, Zhang YY, Guo LX, Liu B, Sun J, Fu QG (2025) Long term protection of silicide coating at 1700 ℃ in air with HfO_2 modification. Corros Sci 255:113122
33. Wang CC, Li KZ, He DY, Shi XH (2020) Evolution behavior of rare-earth yttria modified silicide oxidation-resistant coating at 1700 ℃. J Eur Ceram Soc 40:4419-4427
34. Yu JY, Chen DZ, Xu FD, Wang S, Cui XY, Gong WT, Chen RR (2024) Simultaneous improving high temperature oxidation resistance and room temperature toughness of Nb-Si based alloy via appropriate Ta content addition strategy. Int J Refract Met Hard Mater 124:106800
35. Liu XJ, Luo H, Lu Y, Han JJ, Li J, Guo YH, Huang YX, Wang CP (2017) Thermodynamic Assessment of the Nb-Si-Ta System. J Phase Equilib Diffus 38:897-905
36. He S, Liu Y, Ma Z, Zhu S, Liu L, Mu G, Li Y (2024) Study on anti-ablation properties of HfB_2-$TaSi_2$ coatings prepared by atmospheric plasma spraying. J Alloys Compd 999:175069
37. Xu Y, Zheng W, Dai M, Xu X, Hong D, Zhong X, Niu Y, Zheng X (2023) Effect of $TaSi_2$ addition on long-term ablation behavior of HfB_2-SiC coating. J Eur Ceram Soc 43:5802-5813
38. Xu Y, Dai M, Yu L, Huang S, Zhong X, Niu Y, Zeng Y, Zheng X (2025) Ablation behavior and mechanism of modified HfB_2-SiC coatings. Surf Coat Technol 496:131725
39. Bahr A, Richter S, Hahn R, Wojcik T, Podsednik M, Limbeck A, Ramm J, Hunold O, Kolozsvari S, Riedl H (2023) Oxidation behaviour and mechanical properties of sputter-deposited $TMSi_2$ coatings (TM = Mo, Ta, Nb). J Alloys Compd 931:167532
40. Zhang YF, Liu SN, Zhou XJ, Zhao G, Liu J, Shen HT, Cai ZY, Zhao XJ, Xiao LR (2022) Ultra-high temperature oxidation behavior of ZrB_2/YSZ modified Si-Mo-W coating with a diffusion barrier on niobium alloy. Corros Sci 195:109977
41. Wang Z, Zhang YP, Zhou SH, Wang ZY, Yao YR, Wang AY, Li M, Ke PL (2024) Oxidation resistance of Mo/Cr bilayer coating on Zr alloy in a 1200 ℃ steam environment. Corros Commun 14:49-57
42. Yin L, Ma JY, Yang F, Nie YJ, Meng LX, Wang YZ, Zheng LW, Shi QX, Liang W (2025) Influence of precipitates on the initial oxidation behavior of GH4169 superalloy at 1000 ℃. Corros Commun 19:138-148
43. Dorner F, Sukurma Z, Dellago C, Kresse G (2018) Melting Si: Beyond density functional theory. Phys Rev Lett 121:195701
44. Sekido N, Aizawa R, Ueno S (2019) Effect of Cr Addition on the phase equilibria and oxidation behavior of $NbSi_2$. Mater Trans 60:666-673

45. Tsakiropoulos P (2017) On the Nb silicide based alloys: Part I - The bcc Nb solid solution. J Alloys Compd 708:961-971
46. Ansel D, Thibon I, Boliveau M, Debuigne J (1998) Interdiffusion in the body cubic centered β-phase of Ta-Ti alloys. Acta Mater 46:423-430
47. Roy S, Prasad S, Divinski SV, Paul A (2014) Diffusion pattern in MSi_2 and M_5Si_3 silicides in group VB (M = V, Nb, Ta) and VIB (M = Mo, W) refractory metal-silicon systems. Philos Mag 94:1508-1528
48. Fattah-alhosseini A, Chaharmahali R, Dikici B, Kaseem M (2025) A comprehensive review of plasma electrolytic oxidation (PEO) of tantalum (Ta): Mechanisms, properties, and applications. Int J Refract Met Hard Mater 128:107059
49. Kane KA, Pint BA, Mitchell D, Haynes JA (2021) Oxidation of ultrahigh temperature ceramics: kinetics, mechanisms, and applications. J Eur Ceram Soc 41:6130-6150
50. Luo X, Zhang XX, Yang X, Zuo YM, Huang QZ (2025) Effect of titanium and silicon oxides migration on oxide structure evolution and oxidation mechanism of $(Zr_{0.25}Hf_{0.25}Ti_{0.25}Ta_{0.25})C$-30SiC at 1600 ℃. Ceram Int 51:21936-21950
51. Jiang H, Qiao YQ, Zhang WP, Guo XP, Gao JC, Li LF, Nan X (2026) Temperature-dependent oxidation behavior and interfacial diffusion dynamics of multilayered silicide coating on Nb521 alloy (1200-1500 ℃). Surf Interfaces 86:108689

Figures

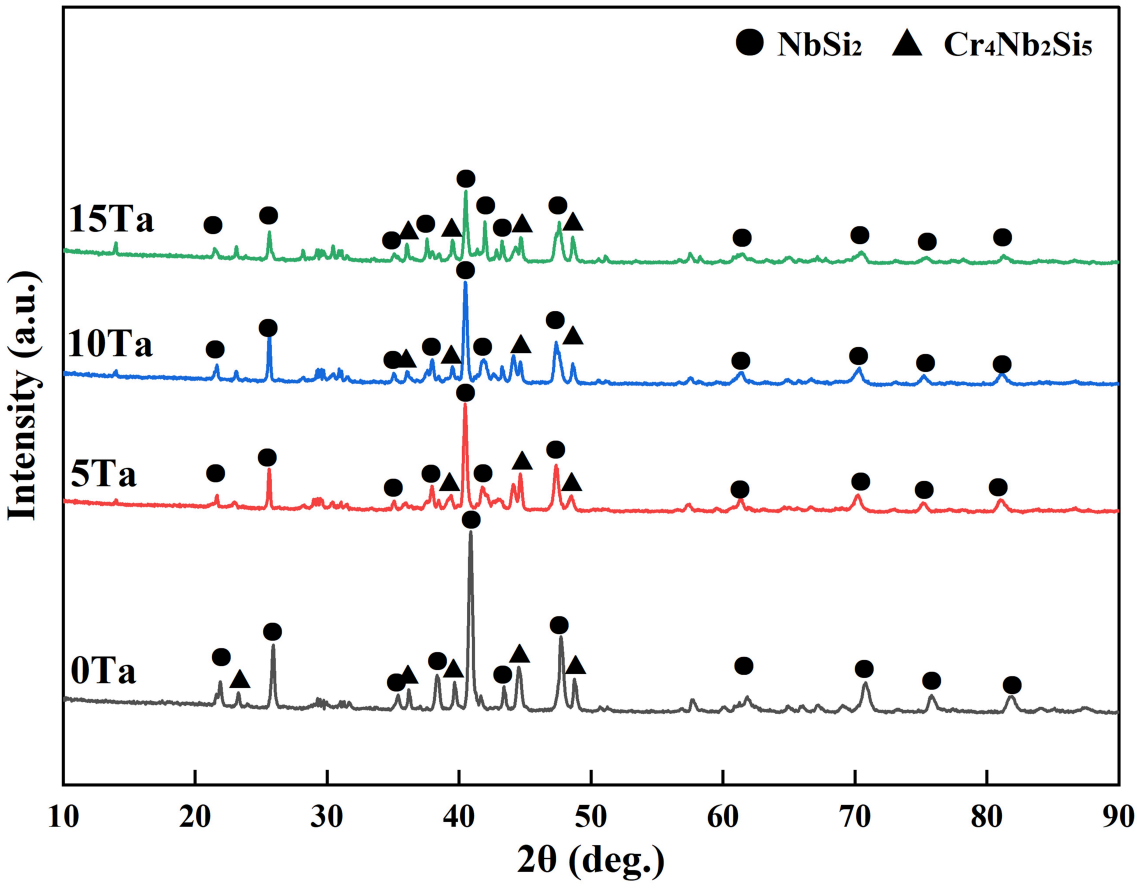


Figure 1

Surface XRD patterns of Cr-Ta-Ti modified silicide coatings with different Ta contents.

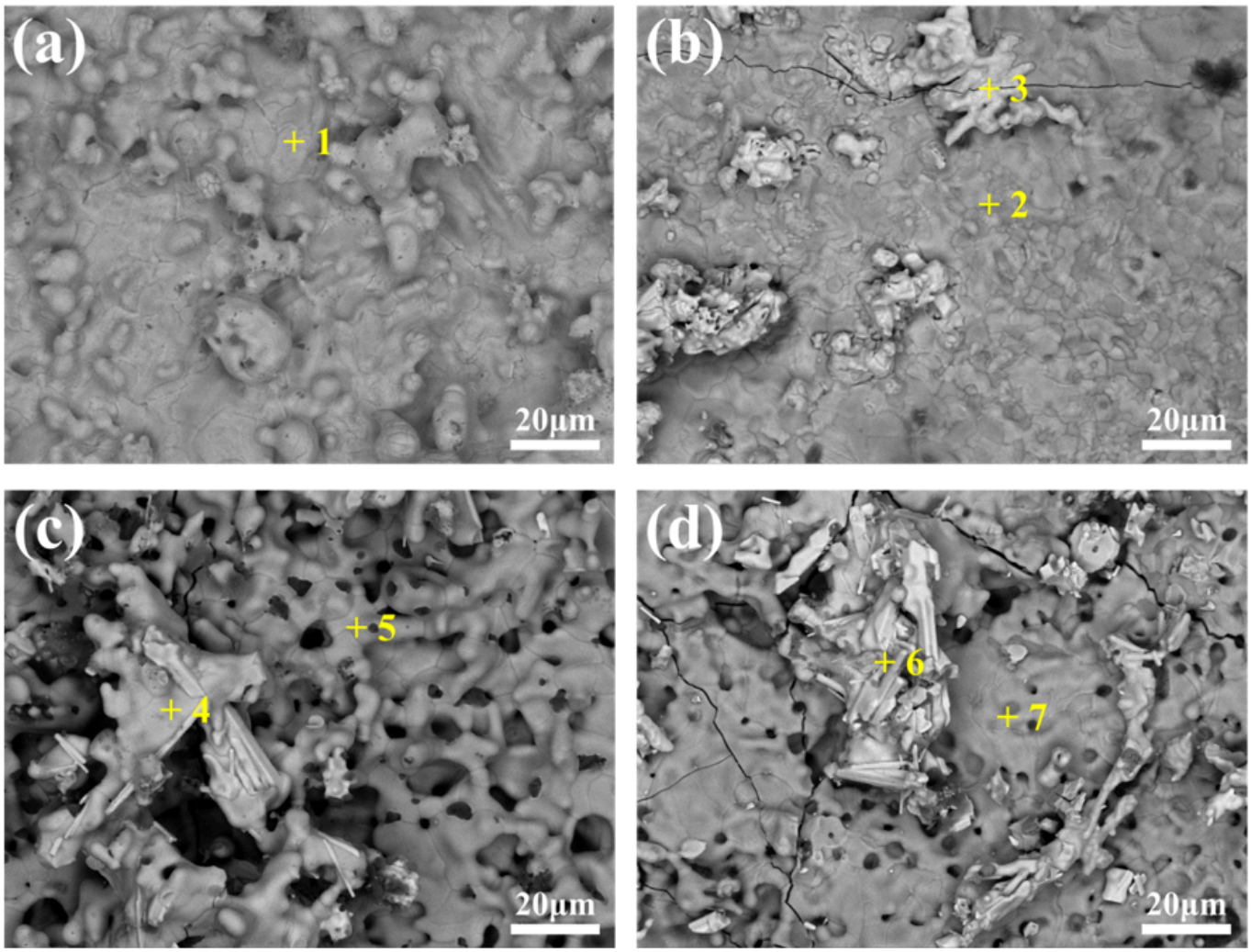


Figure 2

Surface BSE images of Cr-Ta-Ti modified silicide coatings with different Ta contents:

(a) 0Ta, (b) 5Ta, (c)10Ta and (d)15Ta.

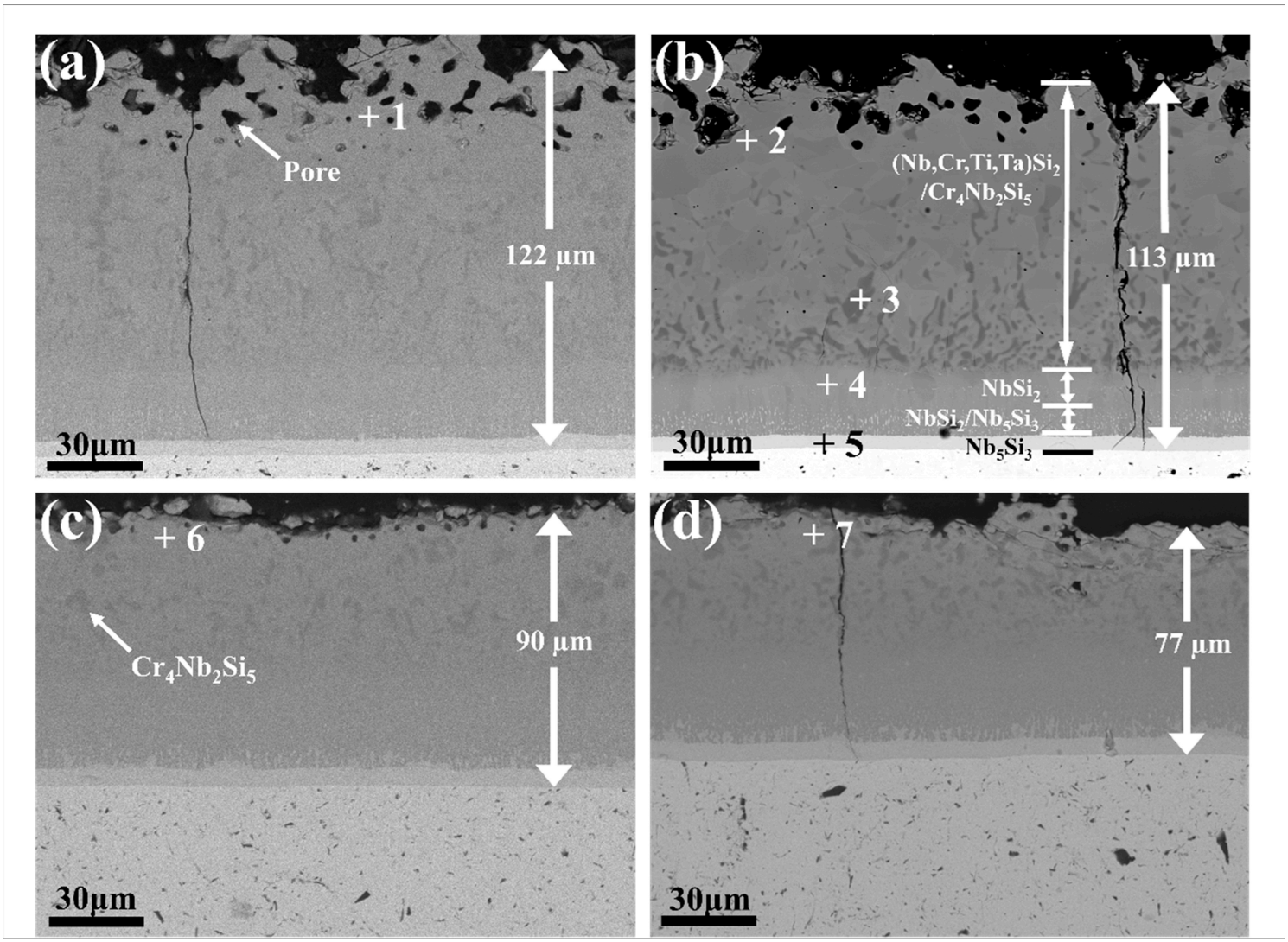


Figure 3

Cross-sectional BSE images of Cr-Ta-Ti modified silicide coatings with different Ta contents: (a) 0Ta, (b) 5Ta, (c)10Ta and (d)15Ta.

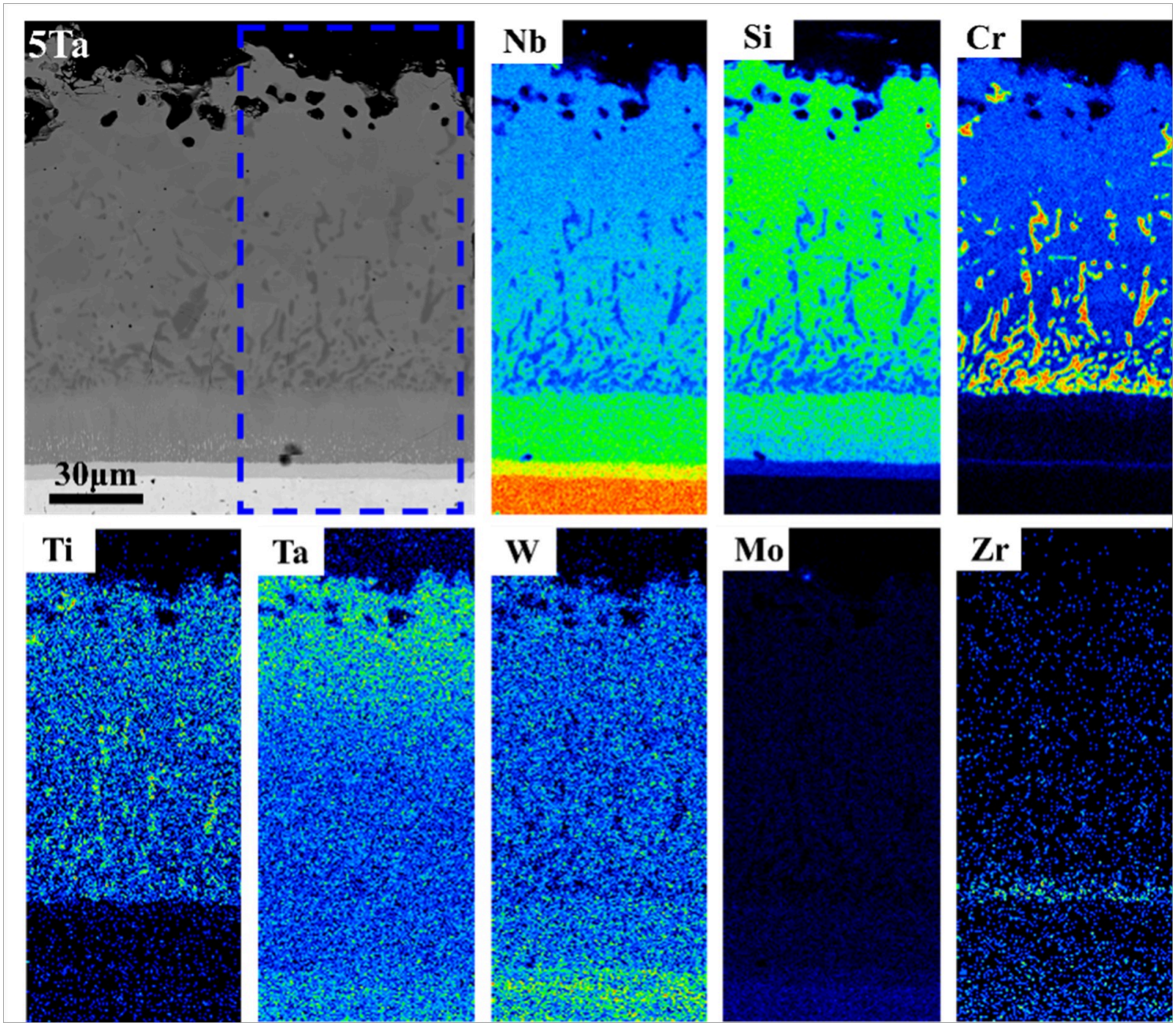


Figure 4

Cross-sectional BSE image of 5Ta coating and the corresponding EPMA elemental mappings.

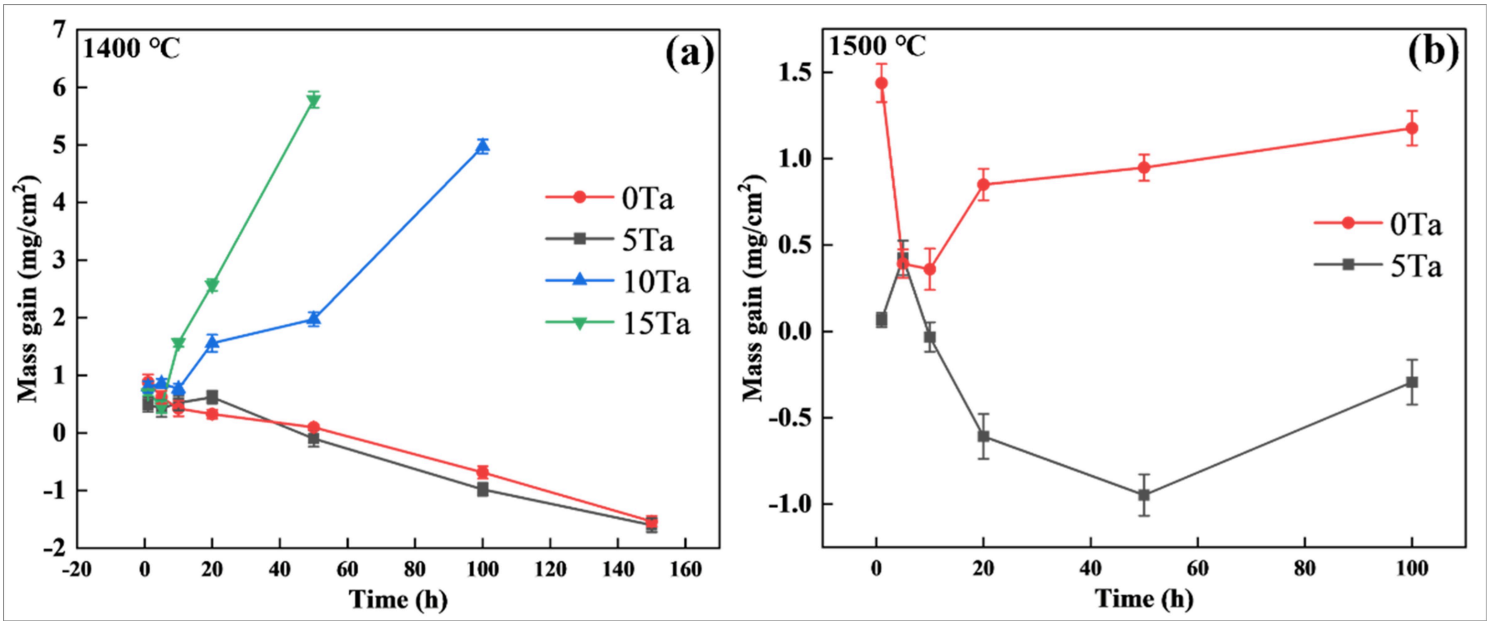


Figure 5

Oxidation mass gain per unit area of the Cr-Ta-Ti modified silicide coatings with different Ta contents after oxidation at 1400 °C and 1500 °C.

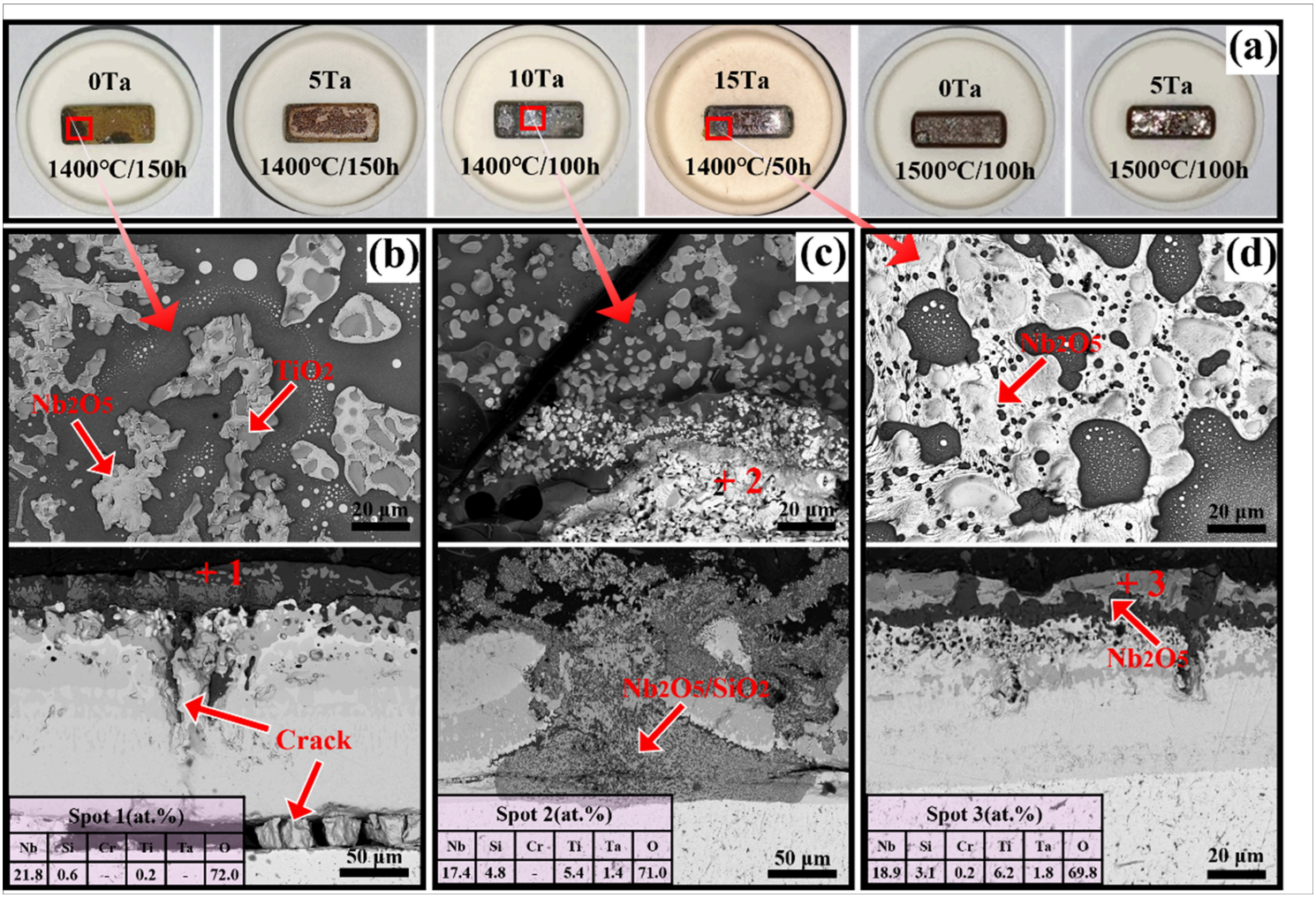


Figure 6

Macroscopic morphologies (a) and corresponding cross-sectional BSE morphologies of the failure regions (b, c, d) of Cr-Ta-Ti modified silicide coatings with different Ta contents after oxidation.

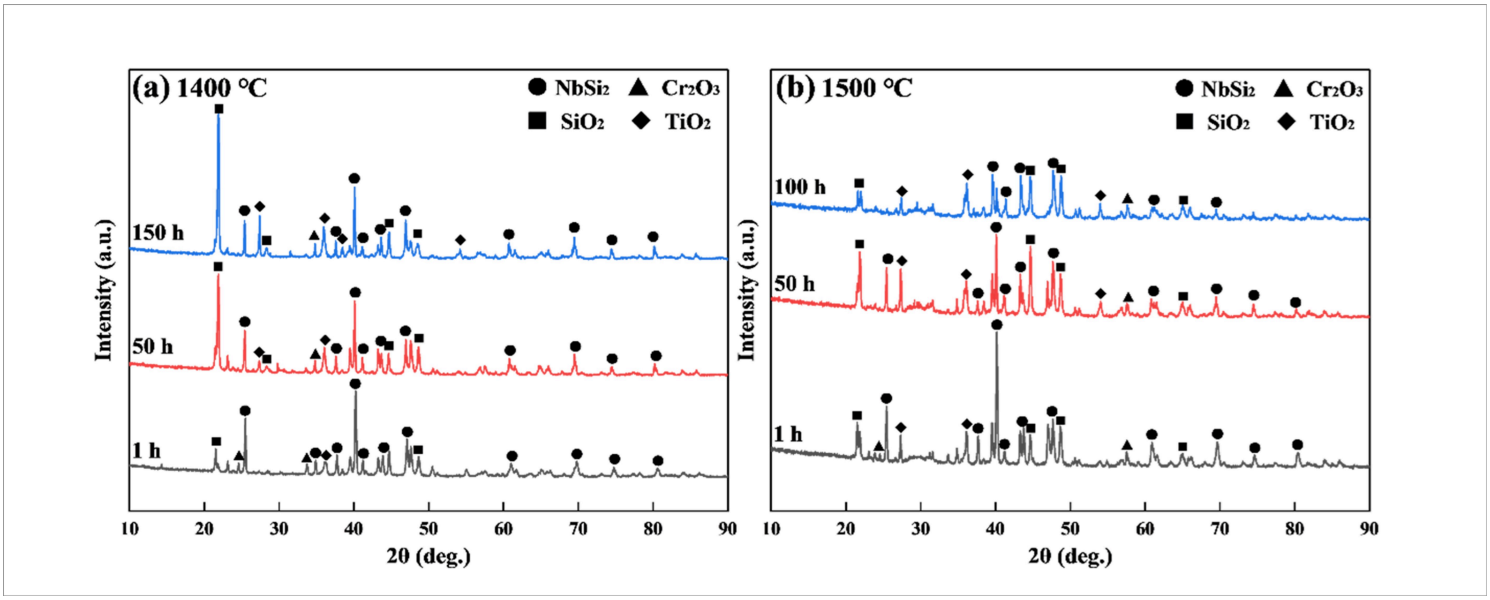


Figure 7

XRD patterns of 5Ta coating after oxidation at 1400 ℃ (a) and 1500 ℃ (b) for different time.

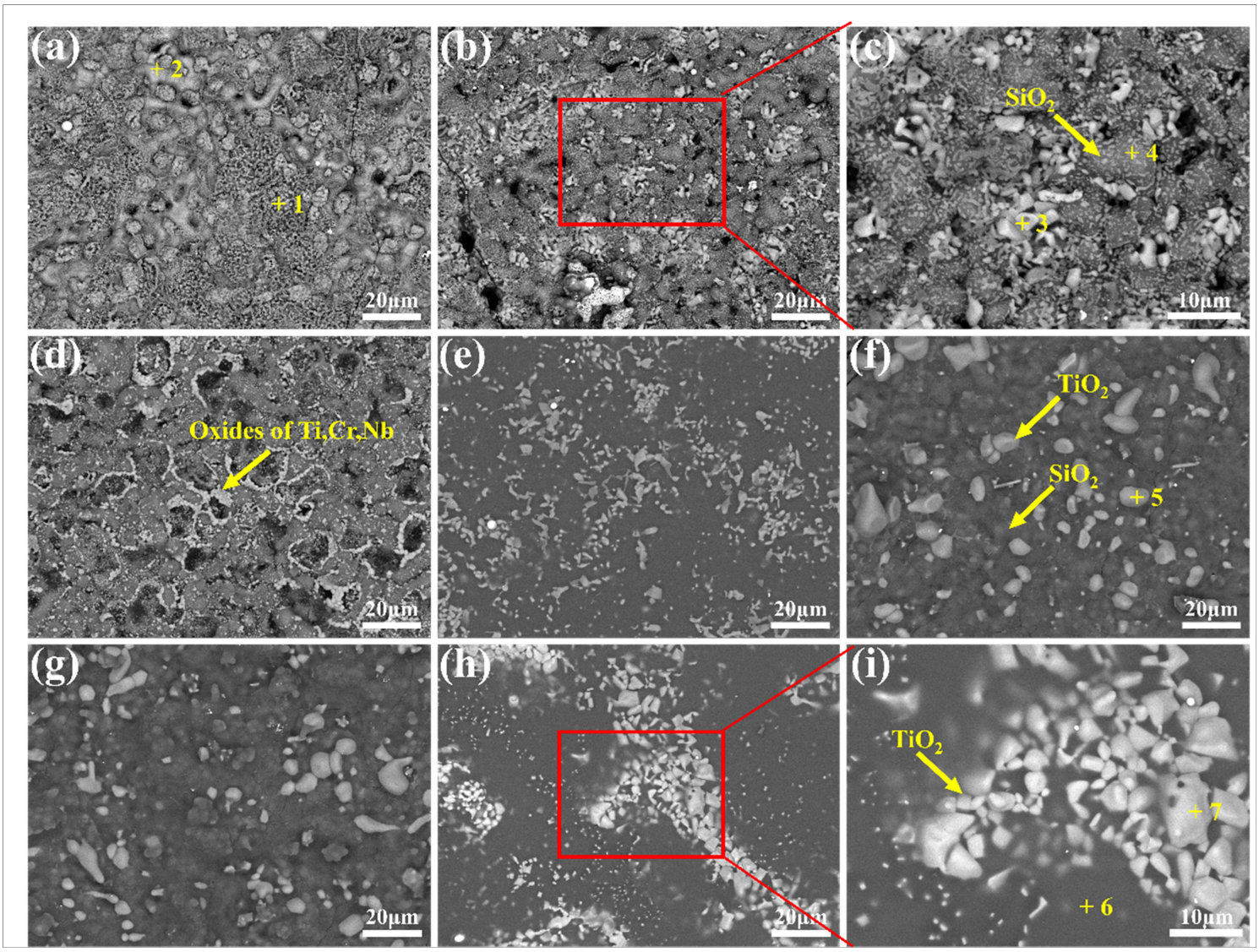


Figure 8

Surface BSE images of 5Ta coating after oxidation at 1400 °C for (a) 1 h, (b,c) 5 h, (d) 10 h, (e) 20 h, (f) 50 h, (g) 100 h and (h,i) 150 h.

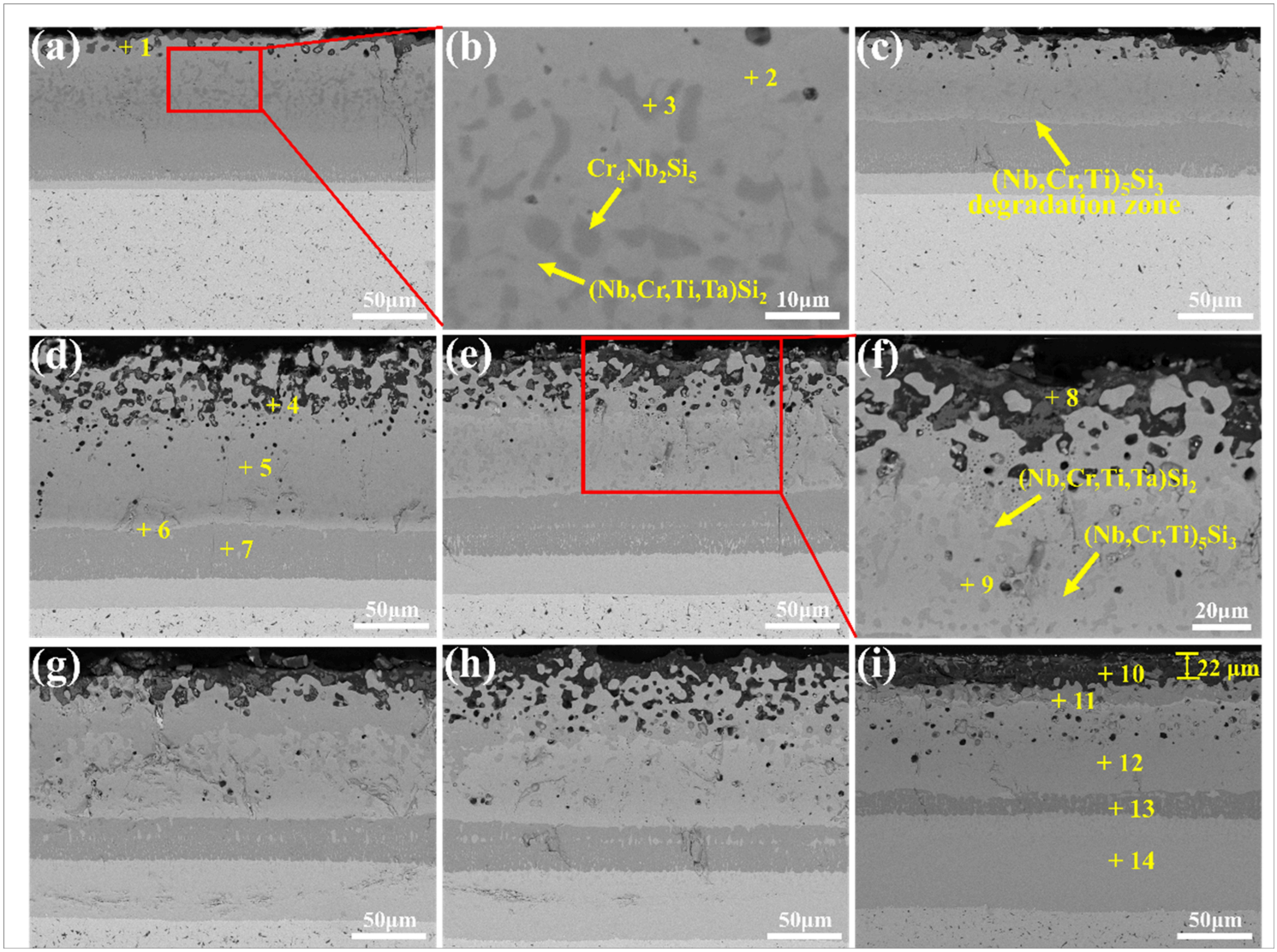


Figure 9

Cross-sectional BSE images of oxide scales for 5Ta coating after oxidation at 1400 ℃ for (a,b) 1 h, (c) 5 h, (d) 10 h, (e,f) 20 h, (g) 50 h, (h) 100 h and (i) 150 h.

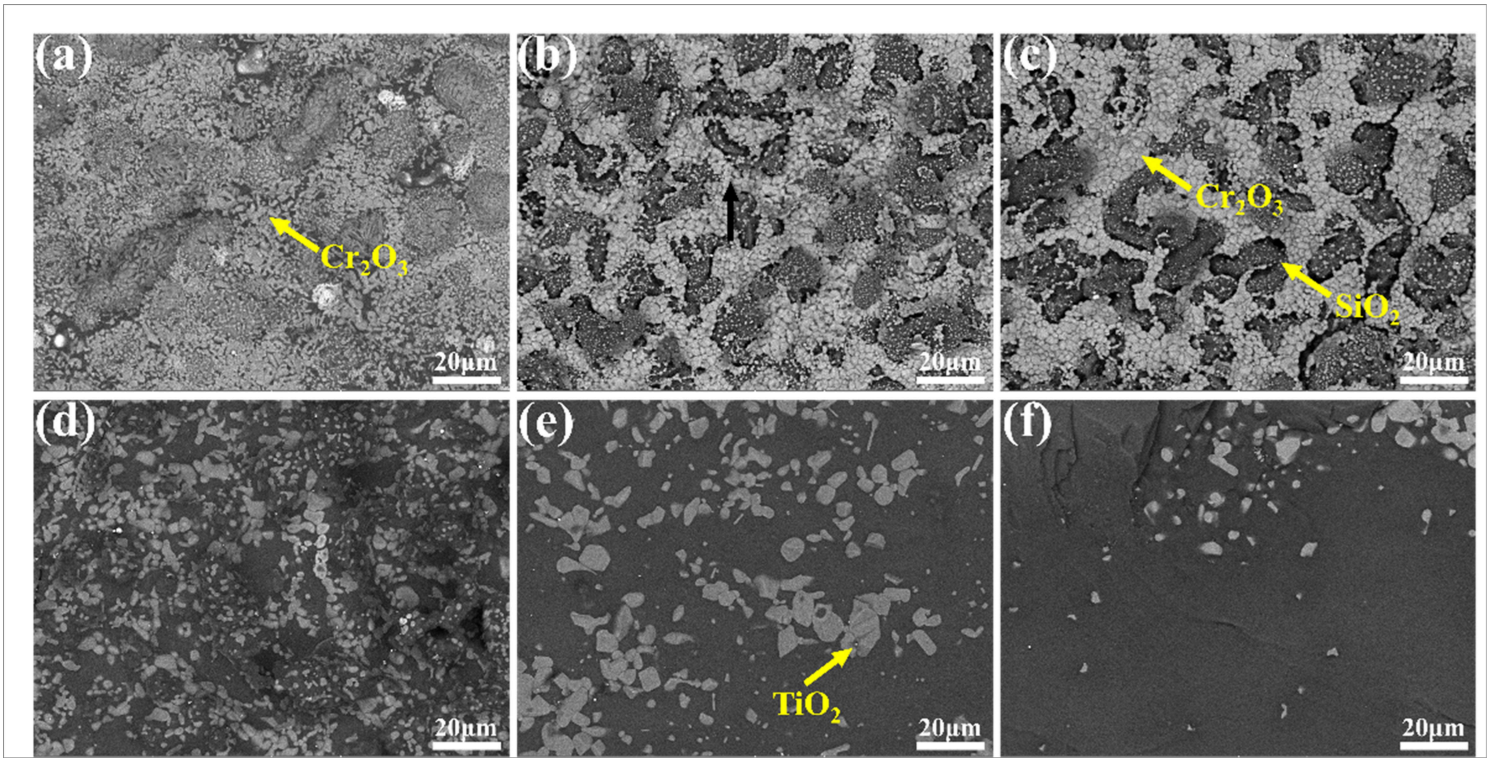


Figure 10

Surface BSE images of 5Ta coating after oxidation at 1500 °C for (a) 1 h, (b) 5 h, (c) 10 h, (d) 20 h, (e) 50 h and (f) 100 h.

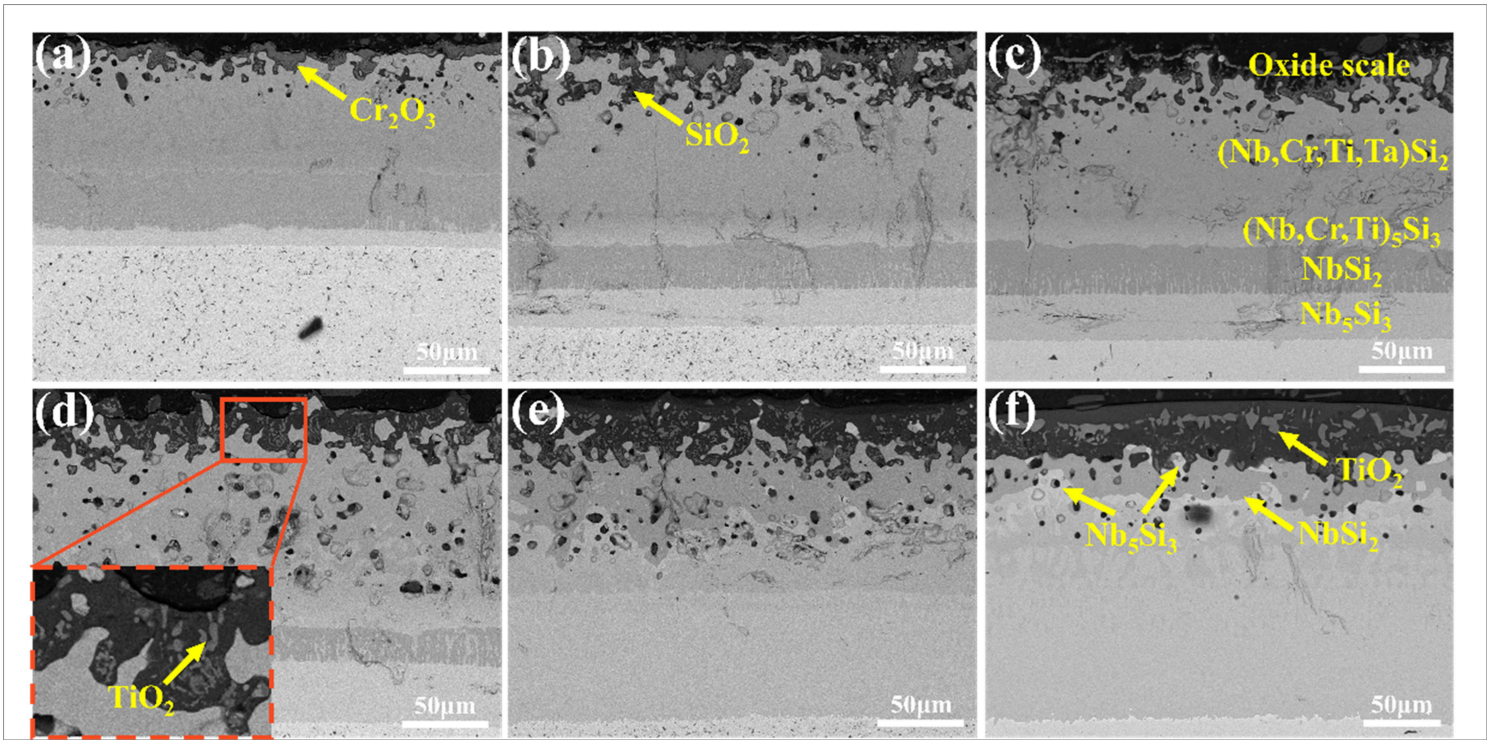


Figure 11

Cross-sectional BSE images of the oxide scales for 5Ta coating after oxidation at 1500 ℃ for (a) 1 h, (b) 5 h, (c) 10 h, (d) 20 h, (e) 50 h and (f) 100 h.

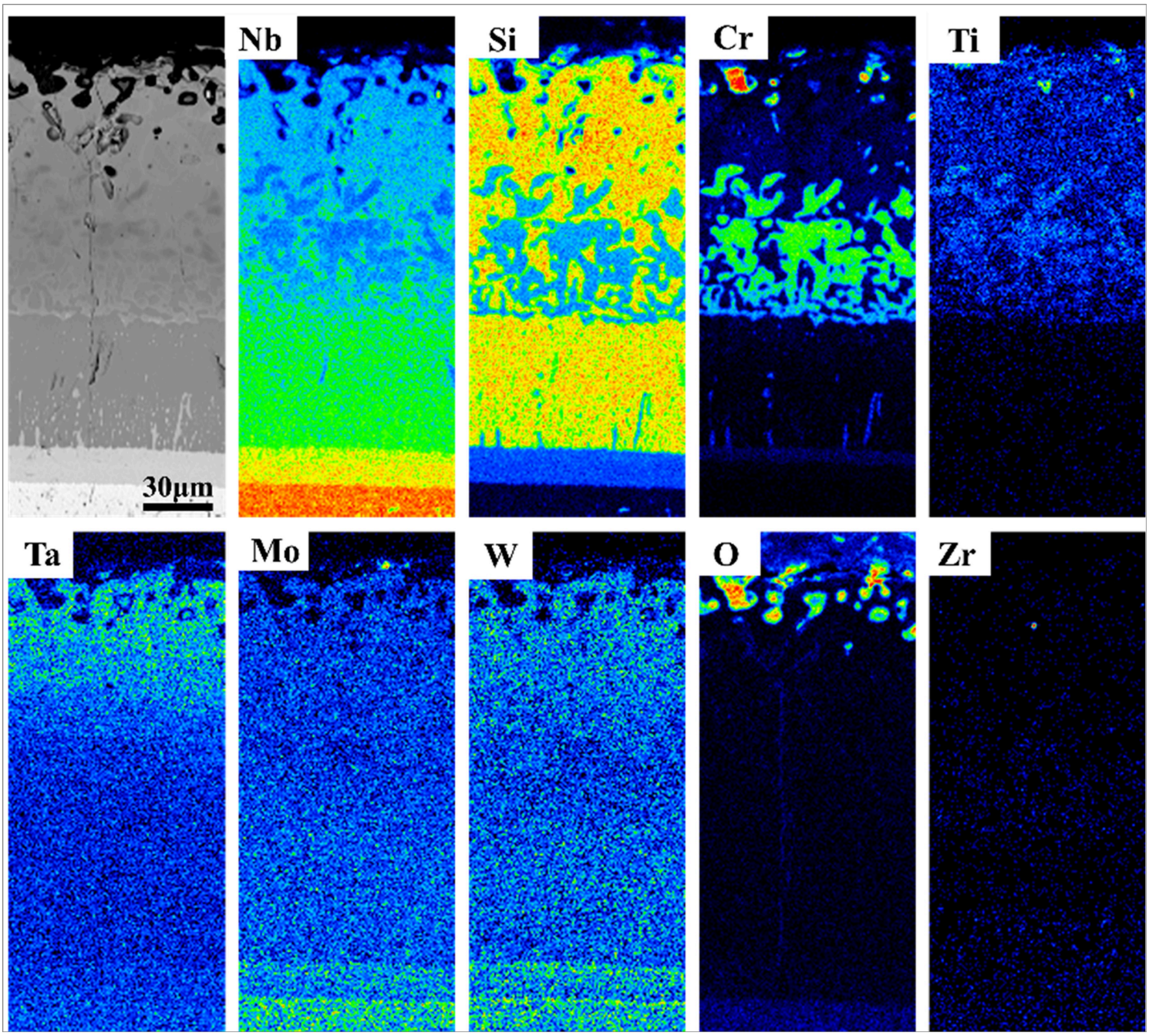


Figure 12

EPMA elemental mappings of 5Ta coating after oxidation at 1500 ℃ for 1 h.

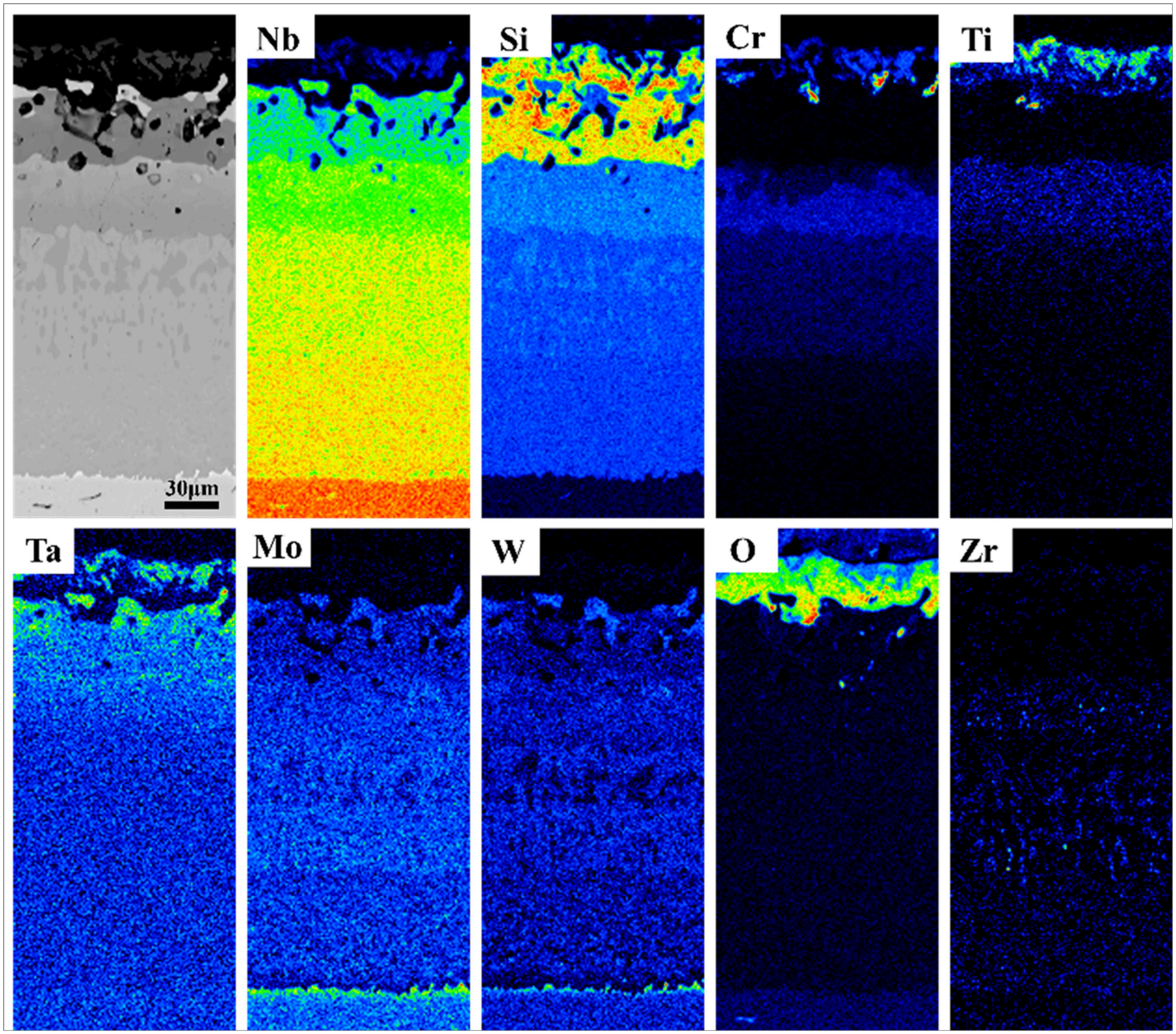


Figure 13

EPMA elemental mappings of 5Ta coating after oxidation at 1500 °C for 100 h.

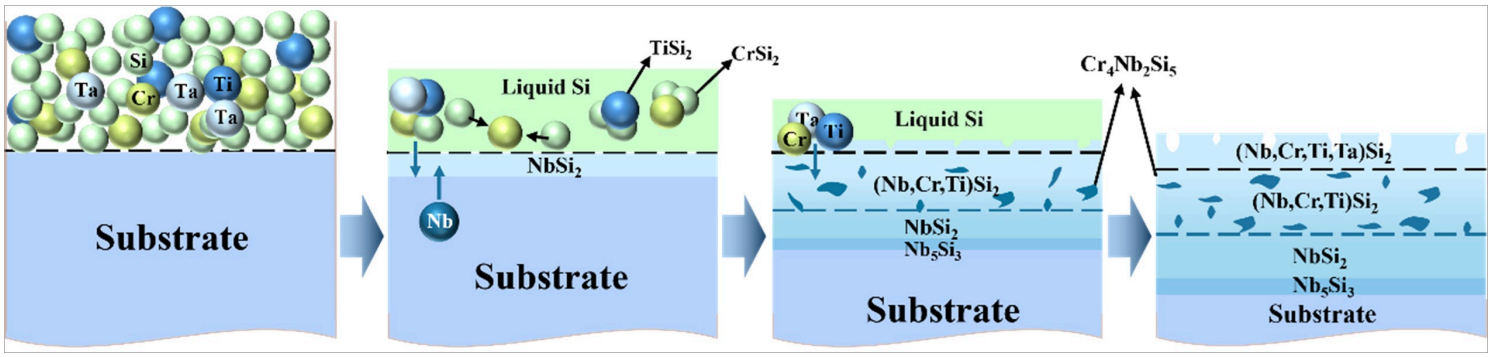


Figure 14

Schematic diagram of the formation mechanism of Cr-Ta-Ti modified silicide coating.

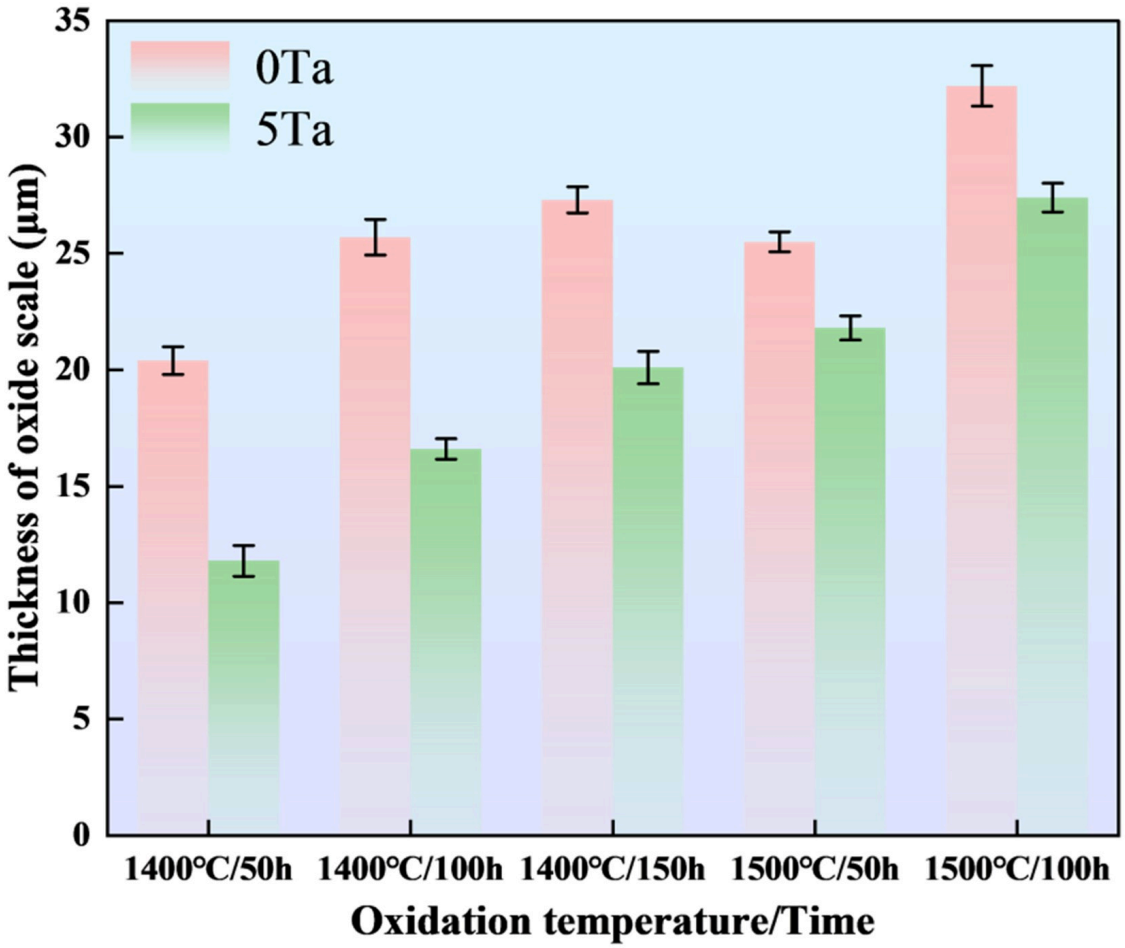


Figure 15

Comparison of oxide scale thickness between 0Ta coating [51] and 5Ta coating.